ACTIVATION ANALYSIS FOR THE CAVITY OF THE PROMETHEUS ICF DESIGN

Insoo Jun and Mohamed Abdou
6288 Boelter Hall, University of California at Los Angeles
Los Angeles, CA. 90024
(310)206-0502

ABSTRACT

Activation analysis for the cavity of the PROMETHEUS ICF design, which uses a wetted first wall protection scheme, has been performed. It has been found that the PROMETHEUS cavity produces about 0.9 Ci/W of thermal power at shutdown after the full 30 years operation, which is about the same amount of radioactivity of other ICF and MCF fusion designs with low activation materials. It was possible, however, to reduce the radioactivity inventory level in the shield by one to three orders of magnitude by introducing a new shield design that uses B_4C, Pb, SiC and water instead of using the conventional concrete shield. Furthermore, the effect of using the spherical and cylindrical modeling on the prediction of radioactivity in the first wall has been studied. It has been found that the cylindrical model with a point neutron source at the center of the cylinder reduces the radioactivity of the short half-life products to about 80% of the values that would be obtained by using purely spherical modeling. Finally, the ^{210}Po problem associated with the use of lead has been analyzed. It is shown that ^{210}Po produced from neutron interactions with lead is more important than that produced from the bismuth impurity (40ppm) existing in lead if the machine is operated over ~1 year.

I. INTRODUCTION

PROMETHEUS, which utilizes a wetted first wall protection scheme, is a laser driven inertial confinement fusion (ICF) reactor conceptual design study led by McDonnell Douglas. One of the main goals of the PROMETHEUS design is to minimize long term radioactivity. The construction materials, particularly in the cavity region have been carefully selected to achieve this goal. For example, the structure in the first wall system, blanket, and shield are all made from SiC/SiC composite, which are currently commercially available and have low long-term radioactivity.

The reactor produces 2773 MW of thermal power, of which 1987 MW are due to fusion neutrons. The D-T fusion targets are imploded by 5 MJ pulses at a rate of 4.2 Hz. The target gain is about 131 MJ, leading to a target yield of 655 MJ.

Fig. 1 depicts a one-dimensional schematics of the cavity. The cavity design of the PROMETHEUS features the use of a thin liquid film, which is supplied through a porous, composite structure of SiC structure material, to endure the shock waves of radiation or heat from the microimplosions. Pb has been chosen due to its many desirable advantages including appropriate temperature ranges and good neutron multiplication.[1] A separate blanket is provided behind the wall protection system for tritium breeding and energy

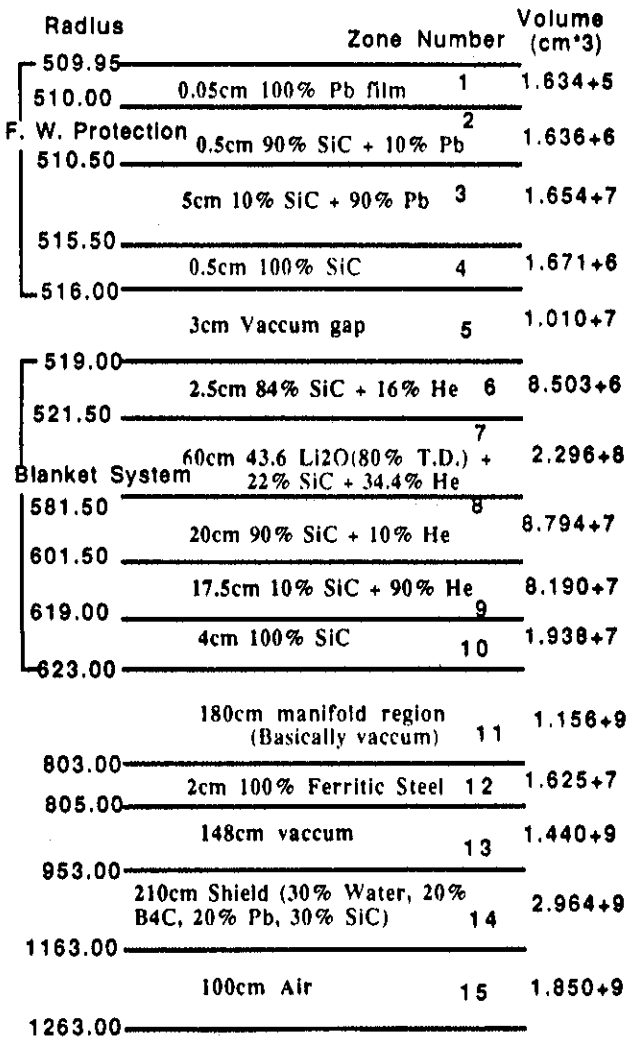

Fig. 1 One dimensional schematics used in ICF design including F.W., Blanket, Shield etc. (Not scaled)

conversion. The blanket uses Li_2O breeder, which also has a low activation characteristic, with SiC structure and Helium coolant. Behind the blanket system, there are vacuum vessel, which is made of 100% ferritic steel, and 210cm of biological shield. The shield consists of $H_2O + B_4C + Pb +$ SiC. Finally, the standard state air is assumed to surround the cavity. More complete reasoning of material selections and a list of design parameters for the cavity can be found in Ref. [1].

In this paper, the results of the activation analysis performed for the PROMETHEUS cavity will be presented. Section II describes the calculation procedures. The results will be discussed in Section III. In Section IV, the problem of ^{210}Po, that is known to be biologically dangerous, will be examined. Finally, concluding remarks will be stated in Section V.

II. CALCULATIONAL PROCEDURE

Fig. 2 shows the calculational procedures as well as the codes and libraries used in calculating the radioactivity. The neutron transport calculation was carried out first by using ANISN[2] to determine the neutron energy spectrum at various locations in the cavity. During ANISN calculation, a P_3S_8 approximation and the neutron/photon cross section data derived from ENDF/B-V[3] have been employed. The problem has been modeled in spherical geometry with materials and dimensions consistent with a cut through the midplane of the cavity. A point source was used at the center of the 510 cm radius cavity. The SIRIUS-M[4] target neutron spectrum was used to represent the source spectrum. The source neutron strength has been obtained as 9.636×10^{20} n/sec by considering the average neutron energy (12.87 MeV) of the SIRIUS-M source spectrum and the neutron power (1987 MW) of the PROMETHEUS design.

The neutron flux obtained from the neutron transport calculation has been used as input to the activation calculation, using the DKRICF[5] code. It has been assumed that the machine is operated for 40 years with 75% availability, which corresponds to approximately continuous 30 years operation. The exact pulse-shaped operation scheme is not considered in this study. It has been reported[6] that even though the employment of a continuous operation scheme underestimates the short-term radioactivity production when compared to the actual pulse-shaped operation scheme, the former scheme produces the same amount of long-term (> 1week after shutdown) radioactivity as the latter scheme does. Therefore, the use of the continuous operation should not affect the long-term radioactivity calculated in this study. It also has to be noted that because the lifetime of the first wall protection system is likely to be limited to about 2 years, the first wall system has been assumed to be irradiated for only 2 years throughout the activation analysis.

III. RESULTS AND DISCUSSIONS

III.A. Radioactivity

Table I summarizes the calculational results as a function of time after shutdown. Table II shows the important reaction products and their originating reactions. Figs. 3 through 5 are the graphical form of the results presented in Table I. In the following, specific quantities given for "activation level" refer to specific radioactivity, i.e., radioactivity per unit volume.

In zone 1, which is 100% Pb film, the activation level at short times after shutdown (0 ~ 1 week) is dominantly governed by the ^{203}Pb (2.17d, $^{204}Pb(n,2n)$) and ^{209}Pb (3.25h, $^{208}Pb(n,\gamma)$). After that, ^{204}Tl (3.78y, $^{204}Pb(n,p)$) takes over the leading role until about 10 years after shutdown. Then, $^{205}Pb(1.9 \times 10^7 y, {}^{204}Pb(n,\gamma)$ or $^{206}Pb(n,2n))$ has the responsibility for the very long-term radioactivity level in this zone. The same behavior of the

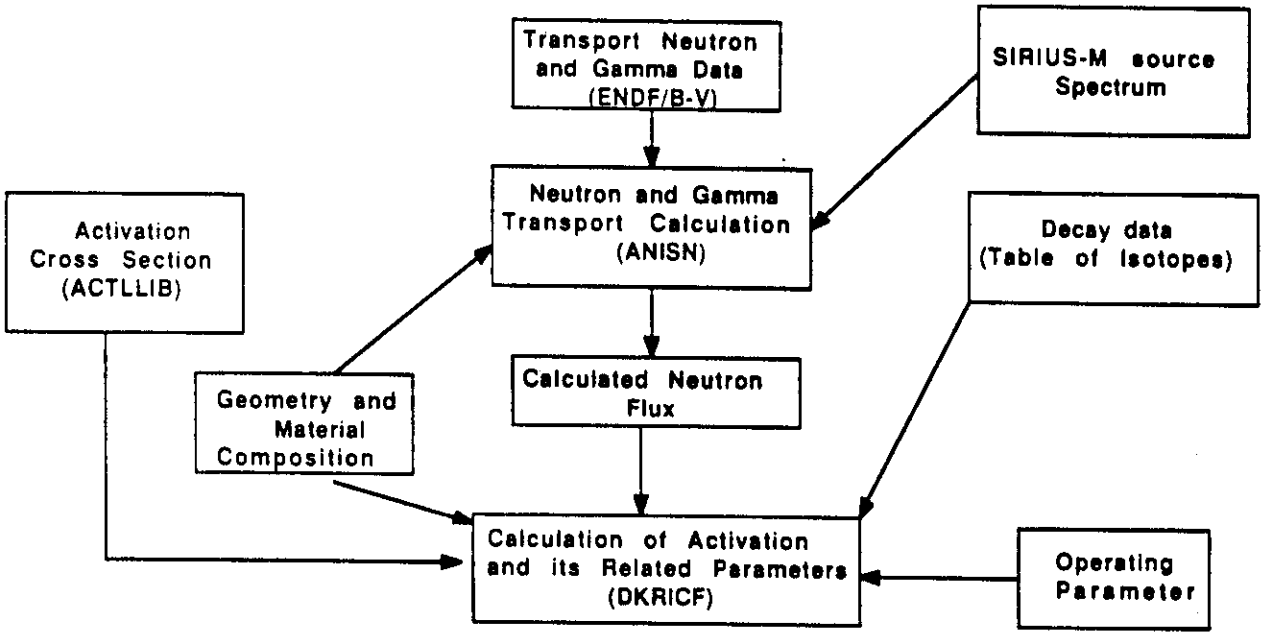

Fig.2 Calculational procedure of radioactivity

Table I Zonal specific radioactivity (Ci/cm^3) as a function of post shutdown times after 30 years full operation. Also shown are the dominating isotopes and their contributions at each time. (Except first wall system which is operated for 2 years)

Post shutdown times	Zone number 1(*)	2(*)	3(*)	4(*)	6	7(+)
0	1.281+1(**) Pb203:59% Pb209:40%	1.093+2 Al28:91%	1.940+1 Al28:37% Pb203:27% Pb209:23%	7.450+1 Al28:93%	5.383+1 Al28:93%	4.791 Al28:77% N16:12%
1 min	1.278+1 Pb203:59% Pb209:40%	7.967+1 Al28:92%	1.676+1 Al28:39% Pb203:31% Pb209:26%	5.429+1 Al28:93%	3.923+1 Al28:93%	2.905 Al28:93%
1 hour	1.165+1 Pb203:64% Pb209:36%	1.305 Pb203:56% Pb209:32%	8.842 Pb203:59% Pb209:41%	1.442-1 Si31:91%	1.014-1 Si31:91%	8.881-3 Si31:93%
1 day	5.560 Pb203:99%	5.458-1 Pb203:99%	3.884 Pb203:99%	3.001-4 Si31:100%	2.139-4 Si31:99%	3.706-5 Si31:51% C14:49%
1 week	8.383-1 Pb203:96%	8.225-2 Pb203:96%	5.846-1 Pb203:96%	2.846-7 Be10:52% C14:48%	3.105-6 Be10:53% C14:47%	1.829-5 C14:99%
1 month	2.398-2 Hg203:81% Tl204:17%	2.348-3 Hg203:81% Tl204:17%	1.647-2 Hg203:81% Tl204:17%	2.846-7 Be10:52% C14:48%	3.105-6 Be10:53% C14:47%	1.829-5 C14:99%
1 year	3.541-3 Tl204:96%	3.473-4 Tl204:96%	2.437-3 Tl204:96%	2.846-7 Be10:52% C14:48%	3.105-6 Be10:52% C14:48%	1.829-5 C14:99%
5 years	1.642-3 Tl204:99%	1.614-4 Tl204:99%	1.132-3 Tl204:99%	2.846-7 Be10:52% C14:48%	3.105-6 Be10:53% C14:47%	1.829-5 C14:99%
10 y	6.632-4 Tl204:98%	6.560-5 Tl204:97%	4.567-4 Tl204:98%	2.846-7 Be10:52% C14:48%	3.105-6 Be10:53% C14:47%	1.829-5 C14:99%
100 y	1.320-5 Pb205:100%	1.653-6 Pb205:78% Be10:13% C14:9%	9.224-6 Pb205:99%	2.827-7 Be10:52% C14:42%	3.081-6 Be10:53% C14:47%	1.807-5 C14:99%
1,000 y	1.320-5 Pb205:100%	1.640-6 Pb205:79% Be10:13% C14:8%	9.224-6 Pb205:99%	2.687-7 Be10:55% C14:45%	2.940-6 Be10:56% C14:44%	1.620-5 C14:99%
10,000 y	1.320-5 Pb205:100%	1.543-6 Pb205:84% Be10:13%	9.224-6 Pb205:99%	1.878-7 Be10:78% C14:22%	2.070-6 Be10:79% C14:21%	5.531-6 C14:98%

(*)2 years operation for first wall system
(**)Read as 1.218×10^{1}
(+)Excluding tritium activation

activation level is found in zone 3, which consists of 10% SiC and 90% Pb, except ^{28}Al (2.24min, ^{28}Si(n,p)) being one of the major contributors at very short times after shutdown. In zones 4, 6, 8, 9, 10, where only SiC is the main material, the activation level in the time span of 0 to ~5min after shutdown is mainly due to ^{28}Al. After most of ^{28}Al decays away, ^{31}Si (2.62h, ^{30}Si(n,γ)) becomes the leading contributor between 1 hour ~ 1 day after shutdown. Then, beyond 1 week after shutdown, ^{10}Be (1.6×10^{6}y, ^{13}C(n,α)) and ^{14}C (5.73×10^{3}y, ^{13}C(n,γ)) are responsible for the activation levels in these zones. Zone 2 (90% SiC and 10% Pb) has the in-between characteristics of pure lead zone and pure SiC zone. Refer to Table I for the specific information on this zone. Activation levels in zone 7, which is the breeding zone, come mostly from the SiC structure and are primary governed by ^{28}Al for the short-term and the ^{14}C for the long- and very long-term after shutdown radioactivity. Note that ^{14}C can be produced by 2 reaction channels in this zone - ^{13}C(n,γ) and ^{17}O(n,α). Also note that tritium activation was not included in this zone since most of tritium will be extracted and processed separately for future use. The activation characteristic of the vacuum vessel zone, which made of ferritic steel, is more complex than the other zones because there are larger number of isotopes involved. Briefly, ^{187}W (23.9h, ^{186}W(n,γ)), ^{55}Fe (2.73y,

Table I Continues

Post shutdown times	Zone number 8	9	10	12	14	15
0	9.187-1 Al28:92%	3.376-2 Al28:90%	2.479-1 Al28:90%	8.308-1 W187:44% Cr51:8% Fe55:27%	1.186-3 Al28:62% T:15% Li8:8%	8.270-17 Cl38:27% S37:25% S35:24% C14:17%
1 min	6.766-1 Al28:92%	2.504-2 Al28:89%	1.885-1 Al28:89%	8.283-1 W187:44% Cr51:8% Fe55:27%	8.323-4 Al28:65% T:21%	7.962-17 Cl38:27% S37:23% S35:25% C14:17%
1 hour	1.244-2 Si31:99%	9.344-4 Si31:99%	6.852-3 Si31:99%	7.840-1 W187:45% Cr51:8% Fe55:29%	2.453-4 T:72% Pb209:17%	4.664-17 S35:42% C14:29% Cl38:16%
1 day	2.821-5 Si31:99%	2.131-6 Si31:99%	1.562-5 Si31:99%	5.628-1 W187:32% Cr51:11% Fe55:40%	1.938-4 T:91%	3.812-17 S35:52% C14:36%
1 week	1.321-7 C14:76% Be10:24%	8.933-9 C14:87% Be10:13%	6.527-8 C14:87% Be10:13%	3.354-1 Fe55:65% Cr51:16%	1.791-4 T:99%	3.697-17 S35:51% C14:37%
1 month	1.321-7 C14:76% Be10:24%	8.933-9 C14:87% Be10:13%	6.527-8 C14:87% Be10:13%	3.003-1 Fe55:77% Cr51:10% Mn54:9%	1.760-4 T:99%	3.316-17 S35:47% C14:41%
1 year	1.319-7 C14:77% Be10:23%	8.933-9 C14:87% Be10:13%	6.527-8 C14:87% Be10:13%	1.883-1 Fe55:92%	1.670-4 T:99%	1.741-17 C14:79% Ar39:15%
5 years	1.319-7 C14:77% Be10:23%	8.926-9 C14:88% Be10:12%	6.502-8 C14:87% Be10:13%	6.277-2 Fe55:99%	1.333-4 T:99%	1.627-17 C14:84% Ar39:15%
10 y	1.319-7 C14:77% Be10:23%	8.926-9 C14:87% Be10:13%	6.502-8 C14:87% Be10:13%	1.729-2 Fe55:99%	1.005-4 T:99%	1.622-17 C14:85% Ar39:15%
100 y	1.308-7 C14:76% Be10:24%	8.840-9 C14:87% Be10:13%	6.450-8 C14:87% Be10:13%	3.243-4 Nb93m:70% Mo93:24%	6.343-7 T:99%	1.557-17 C14:87% Ar39:13%
1,000 y	1.205-7 C14:74% Be10:26%	8.046-9 C14:86% Be10:14%	5.882-8 C14:86% Be10:14%	2.745-4 Nb93m:70% Mo93:23%	3.711-9 C14:60% Be10:23% Pb205:17%	1.238-17 C14:99%
10,000 y	6.118-8 Be10:51% C14:49%	3.443-9 C14:68% Be10:32%	2.518-8 C14:68% Be10:32%	5.809-5 Nb93:55% Mo93:23% Nb94:19%	2.227-9 Be10:39% C14:33% Pb205:28%	4.103-18 C14:100%

$^{56}Fe(n,2n)$), and ^{93m}Nb (13.6y, $^{93}Nb(n,n')^*$) are the important contributors for the short-, long-, and very long-term after shutdown radioactivity, respectively. In the shield zone (zone 14), which is made of $B_4C+H_2O+Pb+SiC$, tritium is the most dominating radionuclide during 1 hour to 100 years after shutdown. Tritium is produced via $^{10}B(n,2\alpha)$ reaction in this zone. The air activation (zone 15), which is assumed to surround the reactor cavity, is also estimated. At shutdown, the activation of air is lower than that of the shield by 14 orders of magnitude. However, the air activation does not decay as fast as the other zones do since the ^{14}C ($T_{1/2}$=5730 years) is the major radionuclide. During 10000 years after shutdown, the air activation decays to only 5% of the activation level at shutdown.

Fig. 6 compares the integrated radioactivity (in Curies) in the first wall, blanket, vacuum vessel, and shield regions.. The following observations are made on the results in Fig. 6: (1) The radioactivity inventory of the total cavity at shutdown is about 2.5×10^9 Curies, which can be translated into ~0.9Ci/W of thermal power. This value is comparable to that in other ICF design studies such as HIBALL[7] or in typical MCF designs such as ITER[8]; (2) The blanket/reflector system has the highest radioactive inventory for both very short-term (< few minutes) and very long-term

Table II Important reaction products resulting from the neutron irradiation of various reactor components in the ICF design

Product	Half-life	Originating Reaction
T	12.3 y	B10(n,2α)
Be10	1.6×10^{6} y	C13(n,α)
C14	5.73×10^{3} y	C13(n,γ)
		N14(n,p), O17(n,α)
N16	7.13 sec	O16(n,p)
Al28	2.24 min	Al27(n,γ) Si28(n,p), Si29(n,np/d)
Si31	2.62 h	Si30(n,γ)
S35	87.5 d	Ar38(n,α)
S37	5.1 min	Ar40(n,α)
Cl38	55.6 m	Ar38(n,p)
Ar39	269 y	Ar38(n,γ), Ar40(n,2n)
Mn54	312.2 d	Fe54(n,p), Fe56(n,t)
Fe55	2.73 y	Fe54(n,γ), Fe56(n,2n)
Nb93m	13.6 y	Nb93(n,γ)*
		Mo92(n,γ)Mo93→Nb93m
		Mo94(n,2n)Mo93→Nb93m
		Mo94(n,2n)*Mo93m→Mo93
		→Nb93m
		Mo95(n,3n)Mo93→Nb93m
Nb94	2.0×10^{4} y	Nb93(n,γ)
		Nb93(n,γ)*Nb94m→Nb94
		Mo94(n,p), Mo95(n,np/d) Mo96(n,t)
Mo93	3.5×10^{3} y	Mo92(n,γ), Mo94(n,2n)
		Mo94(n,2n)Mo93m→Mo93
W187	23.9 h	W186(n,γ)
Hg203	46.6 d	Pb206(n,α), Pb207(n,nα)
Tl204	3.78 y	Pb204(n,p), Pb206(n,t)
Pb203	2.17 d	Pb204(n,2n)
Pb205	1.9×10^{7} y	Pb204(n,γ), Pb206(n,2n)
Pb209	3.25 h	Pb208(n,γ), Bi209(n,p)

(> 100 years) after shutdown. The short term activity is mainly due to ^{28}Al and the long-term is due to ^{14}C and ^{10}Be; (3) The activation level in the first wall protection system does not decay as quickly as the blanket system does since it contains the Pb. In the first wall system, the long-term activities are mainly due to the reaction products from Pb; (4) Even though it has the smallest volume of all systems, the vacuum vessel has the largest activation inventory because of the use of ferritic steel which results in much higher long-term radioactivity than that from the SiC/SiC composite used as the structural material in the other zones.

Also, the radioactivity inventory comparison study between our shield ($B_4C+H_2O+Pb+SiC$) and the conventional concrete shield, which is made of 87% concrete+8% ferritic steel+5% H_2O, has been performed and the results are shown in Fig. 7. As shown, the activation level of the PROMETHEUS shield is always less than that of the concrete shield by one to three orders of magnitude. The employment of ferritic steel could result in higher activation in the conventional concrete shield. The use of B_4C gives lower activation in our shield design since boron is a very strong neutron absorber so that the average population of low-energy neutrons in B_4C shield will be less than that in a concrete shield. The neutron and the photon fluxes during the operation right behind the two different shields are displayed in Figs. 8 and 9, respectively. It is apparent that the B_4C shield blocks or absorbs the large number of lower energy neutrons. The photon flux is also lower by about six orders of magnitude in the B_4C shield. Accordingly, the dose rate behind the B_4C shield will be much less than that behind the conventional concrete shield during reactor operation.

It has to be noted at this point that, by adopting the spherical geometry modeling, the results reported in this paper are conservative. In other words, if we consider the actual cylindrical modeling, the average activation level will be less than the results given here. This is because we have a point neutron source at the center of the cavity so that the neutron flux at position B (Fig. 10) will be less than that at position A by roughly a factor of R_A^2/R_B^2. The average flux incident on the first wall can be obtained as

$$\phi_B = \frac{\phi_A}{[1+(\frac{z}{R})^2]}$$

$$\langle\phi\rangle = \phi_A \frac{\int_0^H \frac{dz}{1+(z/R)^2}}{\int_0^H dz}$$

$$= \phi_A \frac{R}{H}\tan^{-1}(\frac{H}{R}) \qquad (1)$$

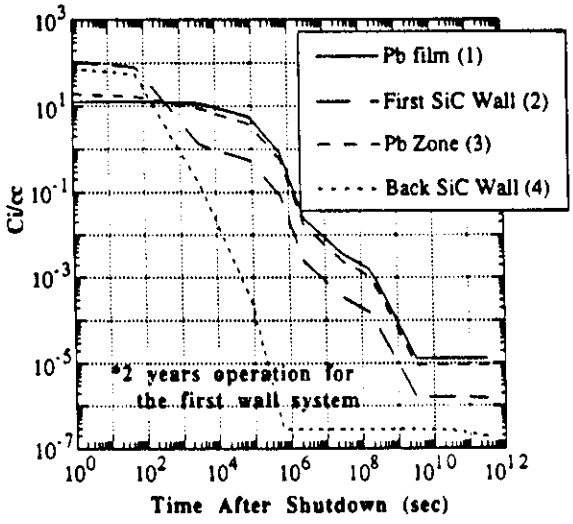

Fig. 3 Specific Radioactivity (Ci/cc) in the First Wall System

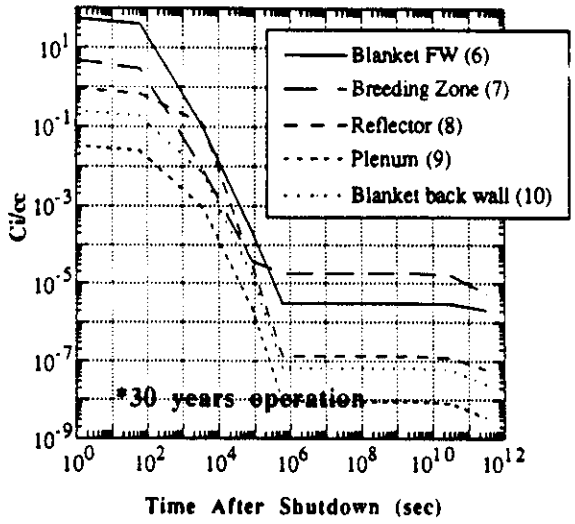

Fig. 4 Specific Radioactivity (Ci/cc) in the Blanket/Reflector System

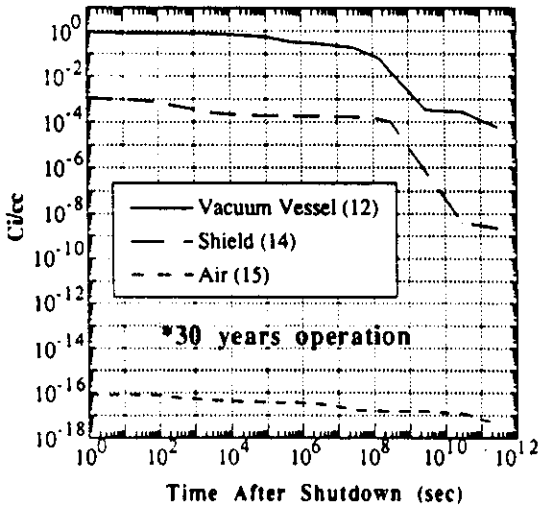

Fig. 5 Specific Radioactivity (Ci/cc) in the Vacuum Vessel, Shield and Air around shield

In the above equation, ϕ_A is the flux at z=0 and H is the half-height of the cylinder. Therefore, if one is to be more accurate, one has to replace the flux term with the Eq. (1) in all the balance equations. As an example, let us consider the most common and simplest reaction/decay chain: A(n,x)B → C. Now we have a following set of equations.

$$\frac{dN_A}{dt} = -\sigma\phi N_A$$

$$\frac{dN_B}{dt} = \sigma\phi N_A - \lambda N_B$$

$$\frac{dN_C}{dt} = \lambda N_B.$$

Then, without the average flux consideration, we have

$$N_B(t) = \frac{\sigma\phi_A N_{A0}}{1 - \sigma\phi_A}\left(e^{-\sigma\phi_A t} - e^{-\lambda t}\right).$$

Now, with the average flux, we have

$$\langle N_B(t)\rangle = \frac{\sigma\langle\phi\rangle N_{A0}}{1 - \sigma\langle\phi\rangle}\left(e^{-\sigma\langle\phi\rangle t} - e^{-\lambda t}\right).$$

Therefore, we get

$$\frac{\langle N_B(t)\rangle}{N_B(t)} = \frac{\langle\phi\rangle}{\phi_A}\,\frac{\lambda - \sigma\phi_A}{\lambda - \sigma\langle\phi\rangle}\,\frac{e^{-\sigma\langle\phi\rangle t} - e^{-\lambda t}}{e^{-\sigma\phi_A t} - e^{-\lambda t}} \qquad (2)$$

Two extreme cases are interesting: (i) $\lambda >> \sigma\phi$ or $\sigma\langle\phi\rangle$ and (ii) $\lambda << \sigma\phi$ or $\sigma\langle\phi\rangle$. In case 1, Eq. (2) becomes

$$\frac{\langle N_B(t)\rangle}{N_B(t)} \sim \frac{\langle\phi\rangle}{\phi_A}\, e^{-\sigma\phi A\left(\frac{\langle\phi\rangle}{\phi_A} + 1\right)t}$$

$$= \frac{R}{H}\tan^{-1}\left(\frac{H}{R}\right) e^{-\sigma\phi_A\left[\frac{H}{R}\tan^{-1}\left(\frac{R}{H}\right) + 1\right]t} \qquad (3)$$

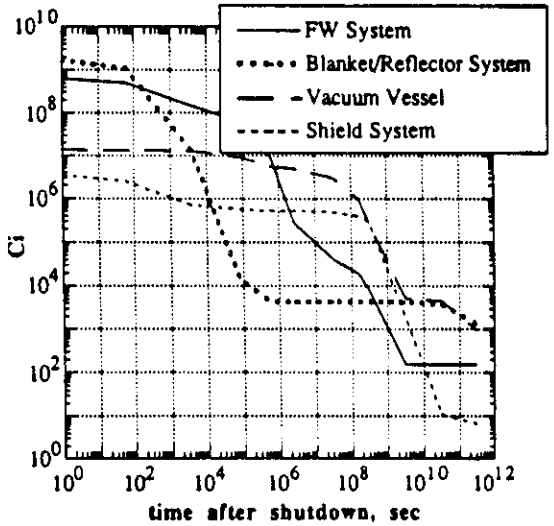

Fig. 6 Integrated radioactivity (Ci) in each component as a function of time after shutdown

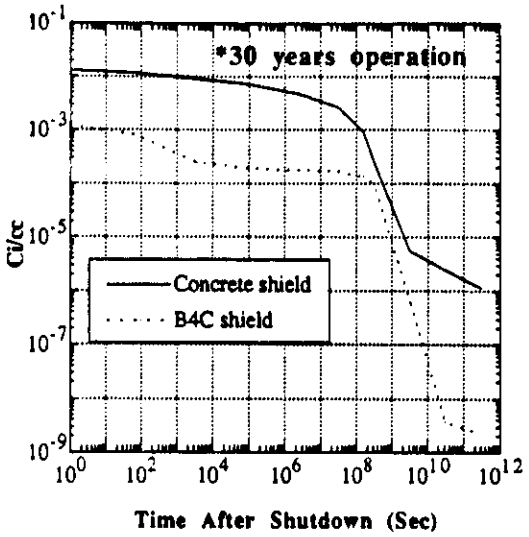

Fig. 7 Comparison of Activation Level between Concrete shield and PROMETHEUS shield

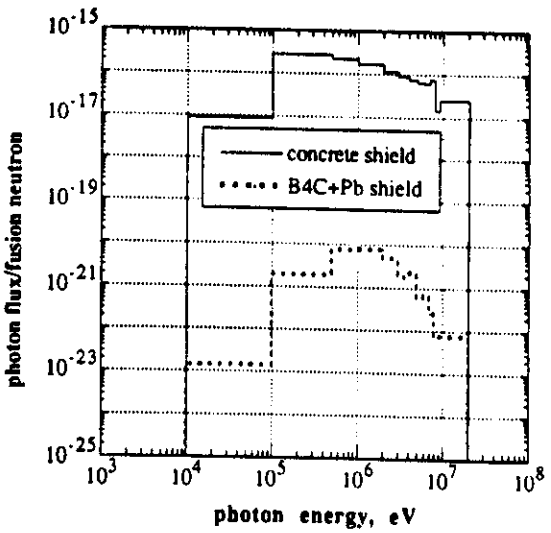

Fig. 9 Photon flux comparison behind two different shields (Concrete shield vs. B_4C + Pb shield)

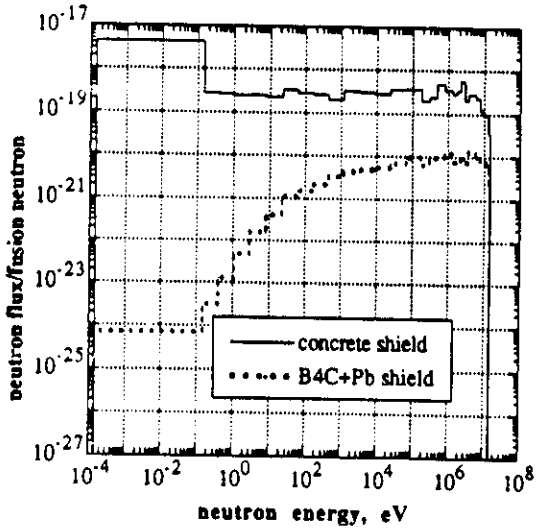

Fig. 8 Neutron flux comparison behind two different shields (Concrete shield vs. B_4C + Pb shield)

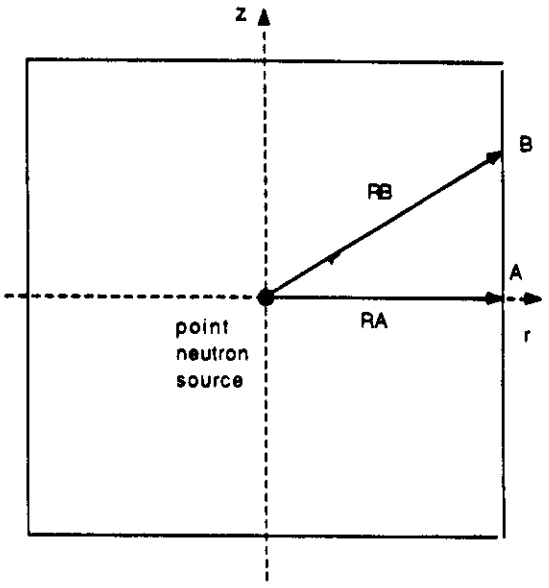

Fig. 10 Cylindrical modeling og the cavity

For case 2, Eq. (2) becomes

$$\frac{\langle N_B(t)\rangle}{N_B(t)} \sim \frac{\langle\phi\rangle}{\phi_A}\,\frac{\sigma\phi_A}{\sigma\langle\phi\rangle}\,\frac{e^{-\lambda t}}{e^{-\lambda t}} = 1,$$

which means that accounting for the difference in the average flux is not necessary for the very long half-life radioactive products. With the typical values of $\phi_A \sim 10^{15}$ n/cm^{2}sec, $\sigma \sim$ 0.1 barn, t ~ 1 year operation, and R=H=5m, $\frac{\langle N_B\rangle}{N_B} \sim 0.78$ for Case 1. Therefore, the average activity in the PROMETHEUS first wall protection system will be about 20% less than the values reported in this paper, specially for the products whose half-lives satisfy the condition of $T_{1/2} \ll \sigma\phi_A$ or $\sigma\langle\phi\rangle$.

III.B. Biological Hazard Potential (BHP)

In addition to the magnitude of radioactivity, the BHP values in each zone have been computed and the results are shown in Figs. 11 through 13 as a function of time after shutdown. The BHP is a measure of the "Biological Hazard" of the radioactivity in various materials.

Fig. 11 shows the BHP values in the first wall system. It shows that the lead containing zones (zone #1 and #3) have

the highest BHP values among the other zones all the times. The products such as ^{209}Pb (3.25h, ^{208}Pb(n,γ)) for short times after shutdown and ^{205}Pb(1.9×10^{7}y, ^{204}Pb(n,γ) or ^{206}Pb(n,2n)) for long times after shutdown are responsible for the high BHP values in Pb zone. In SiC zones (zone #2 and #4), ^{28}Al (2.24min, ^{28}Si(n,p)) is dominating the BHP values for very short times after shutdown. After ^{28}Al decays away, ^{10}Be (1.6×10^{6}y, ^{13}C(n,α)) and ^{14}C (5.73×10^{3}y, ^{13}C(n,γ)) take over the leading role in the SiC zone. But, in general, SiC zone has about 1~3 orders of magnitude lower BHP than the lead zone. Fig. 12 shows the specific BHP values in the blanket and reflector system. Since the SiC is the main material here, every zone in this system shows the same general trend. Furthermore, the

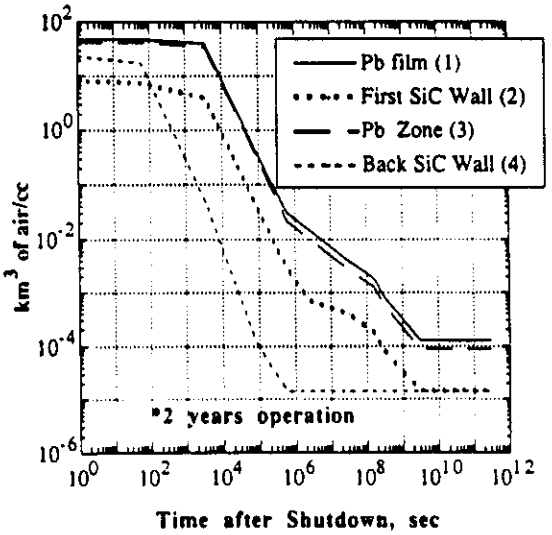

Fig. 11 Specific BHP (km^3 of air/cc) in the First Wall System

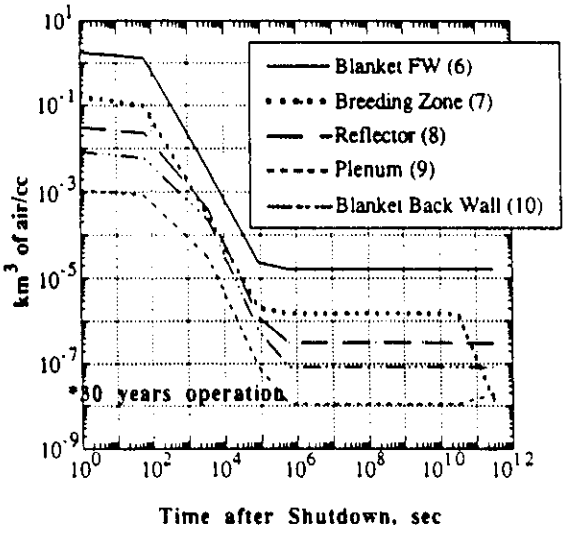

Fig. 12 Specific BHP (km^3 of air/cc) in the Blanket/Reflector System

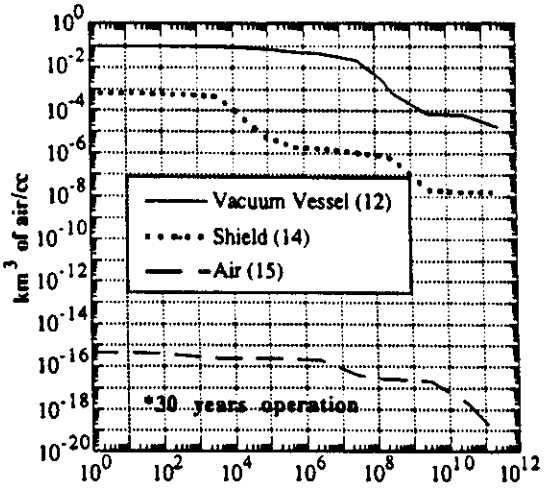

Fig. 13 Specific BHP (km^3 of air/cc) in the Vacuum Vessel, Shield, and Air around shield

deeper the zone is, the lower the BHP values are, because the average neutron flux is less in deeper zone. Fig. 13 shows the specific BHP values in the vacuum vessel, shield, and the air around the cavity. Their general trend is found to be very similar to that of the magnitude of radioactivity discussed before for these zones. However, it has to be noted that ^{54}Mn ($T_{1/2}$=312.2 day, ^{54}Fe(n,p)) is the main contributor for the BHP in the vacuum vessel zone in the time span from shutdown to a few years after shutdown. Other important nuclides include ^{187}W (23.9h, ^{186}W(n,γ)), ^{55}Fe (2.73y, ^{56}Fe(n,2n)), and ^{93m}Nb (13.6y, ^{93}Nb(n,n')*) in the vacuum vessel zone. The BHP in the shield zone is governed by ^{28}Al, T, ^{10}Be and ^{205}Pb for the very short-, long-, and very long-after shutdown times, respectively.

IV. Po-210 PROBLEMS

A particular concern in using lead in high neutron field is the production of ^{210}Po. ^{210}Po is an α-emitter and volatile. Bismuth is a common impurity in natural lead and the neutron capture reaction with ^{209}Bi, which is the only stable nuclide in Bismuth, can result in the production of ^{210}Po: ^{209}Bi(n,γ)^{210}Bi → ^{210}Po →. Other reaction/decay chains which can produce the ^{210}Po are:

^{208}Pb(n,γ)^{209}Pb → ^{209}Bi(n,γ)^{210}Bi → ^{210}Po → : chain #1

^{208}Pb(n,γ)^{209}Pb(n,γ)^{210}Pb → ^{210}Bi → ^{210}Po → : chain #2

In general, there has been a lack in literature of exact estimation of the ^{210}Po production rate from the above 2 reaction/decay chains even though it has important safety implications. In this work, detailed estimation of the ^{210}Po production from the first wall system in the PROMETHEUS design has been made based on the available cross-section and decay data. The necessary cross-section data has been extracted from the activation cross-section library in DKRICF and the decay data in the Table of Radioactive

Isotopes[9] have been used. All three reaction/decay chains are considered. The bismuth impurity in the natural lead has been taken as 40ppm throughout the calculation.

First, the results of radioactivity calculations for ^{210}Po in the lead film zone using DKRICF are presented in Tables III and IV as a function of after shutdown time. Table III shows the radioactivity and Table IV shows the BHP. The results shown in these Tables do not include the effect of build-up of ^{210}Po from neutron interactions with natural lead (chains #1 and #2). Even though the activity level of ^{210}Po is small compared to the other dominant radionuclides, it has rather high BHP values because of the much lower maximum permissible concentration, especially during the period of time from 1 week to a few months after shutdown.

Fig. 14 shows the ^{210}Po build-up from each of the 3 reaction/decay chains described above as a function of irradiation time. It is apparent that the production of ^{210}Po from the bismuth impurity is more important among the 3 chains up to about 1 year irradiation. After that, the chain #1 is mainly responsible for the ^{210}Po production. The chain #2 is the least source of the ^{210}Po until the irradiation time reaches about 10 years. Then the ^{210}Po production from this chain exceeds that from the bismuth impurity. While the ^{210}Po production from the bismuth impurity in lead can be controlled since the bismuth impurity in lead can be reduced with the extra purifying process, we do not have much controls over the production of ^{210}Po from the chains #1 and #2. However, replacing lead every year or so can reduce the production of ^{210}Po from the lead reaction/decay chain. The isotopic tailoring method, which reduces the ^{208}Pb content from the natural lead, can be one solution, but, the extra cost is major concern.

V. CONCLUSIONS

A low activation PROMETHEUS ICF design concept has been proposed and the activation analysis for the complete cavity has been performed in this study. Overall, activation inventory in the whole PROMETHEUS cavity after 30 years continuous operation has been shown to be about same as the activation inventory of the other ICF design or the other MCF design which use low activation materials. However, by employing the low activation B_4C+SiC biological shield in our cavity, we were able to reduce the activation inventory in the shield by an one to three orders of magnitude compared to the activation of the conventional concrete shield. Furthermore, since boron is a strong neutron absorber, the flux levels for neutrons and photons behind the shield during the operation have been significantly lowered in our design compared to the concrete shield design.

The effect of spherical modeling of the cavity during calculations, instead of the actual cylindrical geometry, has also been examined. Results show that the spherical modeling overestimates the activation level in the first wall system by about 20% compared to the values that would be obtained when using the cylindrical modeling. Finally, the ^{210}Po problem has been investigated in the first wall system. The results show that it is important to calculate ^{210}Po productions from neutron interactions with natural lead as well as from neutron reactions with the bismuth impurity. ^{210}Po production from natural lead was found to be more contributing than Po^{210} production from bismuth impurity if the machine is to be operated for longer than about 1 year.

REFERENCES

1. M. S. TILLACK, M. Z. YOUSSEF, M. A. ABDOU, et. al., " Initial Design of the PROMETHEUS

Table III Activity (Ci/cm^3) of ^{210}Po with other dominating nuclides in the Pb film

	total	most dominant	second dominant	third	fourth	^{210}Po
at shutdown	6.897	Pb203: 3.977	Pb209: 2.853	Hg205: 4.362-2[(a)]	Hg203: 1.611-2	1.054-4
1 min	6.879	Pb203: 3.976	Pb209: 2.309	Hg205: 3.844-2	Hg203: 1.641-2	1.054-4
1 hour	6.255	Pb203: 3.924	Pb209: 2.309	Hg203: 1.610-2	Tl204: 7.576-3	1.054-4
1 day	2.930	Pb203: 2.889	Pb209: 1.789-2	Hg203: 1.588-2	Tl204: 7.570-3	1.053-4
1 week	4.467-1	Pb203: 4.243-1	Hg203: 1.452-2	Tl204: 7.546-3	Pb205: 1.390-4	1.040-4
1 month	1.829-2	Hg203: 1.032-2	Tl204: 7.460-3	Pb203: 2.719-4	Pb205: 1.390-4	9.400-5
1 year	6.538-3	Tl204: 6.304-3	Pb205: 1.389-4	Hg203: 1.099-4	-	1.756-5

(a) Read as 4.362×10^{-2}

Wetted Wall IFE Reactor Cavity," UCLA-FNT-51, October (1991)

2. W. W. ENGLE, JR., " User's Manual for ANISN, A One Dimensional Discrete Ordinates Transport Code with Anisotropic Scattering," K-1693, Oak Ridge Gaseous Diffusion Plant (1967)

3. R. R. KINSEY, Compiler, " Evaluated Neutron Data File, ENDF/B-V," ENDF Summary Documentation, ENDF-201, 3rd Edition, BNL (1979)

4. B. BADGER, S. I. ABDEL-KHALIK, H. M. ATTAYA, et. al., " SIRIUS-M: A Symmetric Illumination, Inertially Confined Direct Drive Materials Test Facility," UWFDM-711 (1986)

5. D. L. HENDERSON and OSMAN YASAR, " DKRICF: A Radioactivity and Dose Rate Calculation Code Package," UWFDM-714 (1986)

6. H. Y. KHATER AND M. E. SAWAN, " Dose Rate Calculations for a Light Ion Beam Fusion Laboratory Microfusion Facility," UWFDM-809 (1989)

7. B. BADGER, F. ARENDT, K. BECKER, et. al., " HIBALL: A Conceptual Heavy Ion Beam Driven Fusion Reactor Study," UWFDM-450 (1981)

8. H. ATAYA, Y. GOHAR, and D. SMITH, "US-ITER Activation Analysis," Fusion Technology, 19, 1837 (1991)

9. E. BROWNE and R. FIRESTONE, "Table of Radioactive Isotopes," Jone Wiley and Sons (1986)

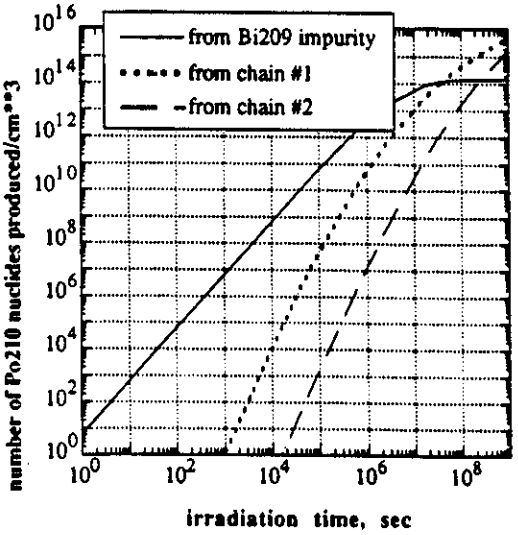

Fig. 14 Po^{210} production from natural lead subjected to the first wall condition of PROMETHEUS design

Table IV BHP (km3 of air/cm^3) of ^{210}Po with other dominating nuclides in the Pb film

	total	most dominant	second dominant	third	fourth	^{210}Po
at shutdown	2.863+1	Pb209: 2.853+1[(a)]	Pb203: 6.634-2	-	-	1.756-2
1 min	2.853+1	Pb209: 2.841+1	Pb203: 6.628-2	-	-	1.756-2
1 hour	2.319+1	Pb209: 2.310+1	Pb203: 6.542-2	-	-	1.756-2
1 day	2.627-1	Pb209: 1.789-1	Pb203: 4.815-2	-	-	1.756-2
1 week	4.166-2	-	-	-	-	1.734-2
1 month	3.053-2	-	-	-	-	1.566-2
1 year	1.136-2	Tl204: 7.007-3	-	-	-	2.922-3

(a) Read as 2.853×10^1